Surface Science 298 (1993) 215–224
North-Holland

surface science

Temperature dependence and anharmonicity of phonons on Ni(110) and Cu(110) using molecular dynamics simulations

D.D. Koleske [1] and S.J. Sibener [2]

Department of Chemistry and The James Franck Institute, The University of Chicago, 5640 South Ellis Avenue, Chicago, IL 60637, USA

Received 15 June 1993; accepted for publication 22 July 1993

Molecular dynamics simulations were performed for Ni(110) and Cu(110) using Finnis–Sinclair model potential. During the simulations the temperature dependencies of the mean-square displacements (MSD), the layer-by-layer stress tensors, and the surface phonon spectral densities were measured. A more pronounced increase in the MSD perpendicular to the atomic rows was observed as the temperature was increased as compared to either the other in-plane direction or along the surface normal. Also, at each temperature studied, the MSD along the direction normal to the surface were always larger in the second layer than in the first. Our calculations reveal that the surface phonon frequencies all decrease linearly with increasing temperature. Moreover, the surface phonon linewidths increase linearly with T at low T, and then exhibit an increased sensitivity to temperature variation, changing from a T to T^2 dependence, approximately 150° before the onset of defect creation at the surface. These simulation results imply that the Ni(110) and Cu(110) surfaces do not extensively roughen before the onset of adatom-defect formation, and, in confirmation of experimental findings, that the rapid decrease of specular intensity for helium or electron scattering at elevated temperatures is due to the influence of anharmonicity in the surface potential.

1. Introduction

Many recent studies on the (110) faces of fcc metals have focussed on the changes in surface structure that occur as the surface is heated, specifically how the surface order is lost on the way to the melting transition [1–15]. These studies have predominantly concentrated on structural changes at high temperatures, for example, the proliferation of steps as roughening occurs [1–4].

In addition to structural changes, surface vibrational spectroscopies such as high resolution electron energy loss spectroscopy (HREELS) and helium atom scattering (HAS) have recently been used to measure the thermal dependence of surface vibrations [9,12–15]. For relatively open (110) surfaces, these studies suggest that temperature (T) induced structural changes such as roughening and melting cannot be considered independently from the influence that anharmonicity in the surface potential can exert on surface vibrational properties at elevated temperatures [9,12–15].

For example, two differing interpretations that have been proposed to explain high-T diffraction experiments on Ni(110) and Cu(110) where a rapid decrease in specular diffraction intensity was observed at approximately half of the melting T [1–9]. One interpretation for this rapid specular intensity decrease at elevated temperature is that the surface structure is changing, accompanied by a roughening transition. Another possibility is that the surface vibrations are sampling the anharmonic region of the surface potential.

Previous X-ray studies have measured the decrease in specularly reflected signal on Cu(110)

[1] Current address: IBM, T.J. Watson Research Center, P.O. Box 218, Yorktown Heights, NY 10598, USA.

[2] 1992/93 Visiting Fellow, Joint Institute for Laboratory Astrophysics, University of Colorado, Boulder, CO 80309-0440, USA.

near $T = 870$ K [1]. In the low temperature regime the extent of this decrease could be attributed to the expected "Debye–Waller" type increase in the mean-square displacements (MSD) normal to the surface [1]. However, at elevated temperatures a stronger than predicted Debye–Waller scattering attenuation was observed. This was attributed to an increase in the step density at the surface, and the concomitant presence of more loosely vibrating surface atoms of lower coordination. However, the possible role that anharmonicity might be exerting on the surface dynamics at elevated T could not be ruled out [1]. Related changes in the MSD for Ni(110) have also been observed in a high resolution low energy electron diffraction (LEED) study at about half the melting T, T_m, of Ni [8].

A similar drop in elastically scattered specular intensity was also observed during HAS experiments on Cu(110) [9]. As the surface was heated up to ~ 700 K the reflected He signal dropped "rapidly" with increasing T [9]. However, HAS measurements of the diffuse elastic intensities on Cu(110) did not show an increase in the number of steps or defects up to $T = 900$ K [9]. The HAS results indicated that no roughening occurs up to 900 K for this interface, and that the rapid decrease in specularly reflected intensity should be attributed to anharmonicity in the surface potential [9]. Molecular dynamics (MD) simulations tend to support these findings, with no increase in step density of adatom–vacancy pair defects being observed using effective-medium-theory (EMT) based potentials up to $T = 1000$ K [11]. This has also been confirmed for Cu(110) using the embedded atom method (EAM) up to $T = 900$ K [10], and for Ni(110) using EAM potentials up to 1400 K [16].

In another study of anharmonic contributions to the surface phonon dynamics, Armand and coworkers have examined the one-phonon and multiphonon contributions to inelastic HAS intensities as a function of T for Cu(110) [17] and Cu(001) [18]. In both of these studies the attenuation of the elastically reflected specular beam and inelastic intensities were calculated using matrix elements which included phonon interactions up to third order, i.e. terms proportional to T^2 [17]. They observed that at low T the MSD are influenced by phonon–phonon scattering terms proportional to T, while as T nears 600 K the T^2 terms become increasingly significant. Recently, we simulated the dynamical behavior of a (110) surface using Lennard-Jones (LJ) potentials and observed that the phonon linewidths are proportional to T at low T, but that they become proportional to T^2 at about 20%–30% of the melting T [19,20]. A sharp rise in the surface phonon linewidths have also been observed in the EAM and EMT simulations of Cu(110) near 600 and 550 K, respectively [10,11]. These simulations have established that anharmonicity in the surface potential becomes more influential in the surface lattice dynamics at higher T. However, an abrupt change in T-dependence from linear to quadratic for surface phonon linewidths has not been clearly resolved.

In this paper we demonstrate that the surface phonon linewidths do exhibit an abrupt change from a linear to quadratic dependence on T, and that this change in the dynamics occurs $\sim 150°$ before the onset of defect creation. We present the T dependence of the Ni(110) and Cu(110) surface phonon spectral densities at $\bar{X}$, $\bar{Y}$ and $\bar{S}$ for both the first and second layers. Also presented are the T dependencies of the layer-by-layer MS displacements and some brief comments on surface stress. These quantities are then compared to the T-dependent frequencies and linewidths measured by Baddorf and Plummer using HREELS [12,13], as well as to the results from simulations which utilized other model potentials, namely EAM and EMT potentials [10,11].

2. Simulation results

The details of the molecular dynamics simulation method we employ have been previously discussed [19,20]. We use Finnis–Sinclair (FS) model potentials [21] with the long-range potential parameters of Sutton and Chen [22]. The potential parameters used by Sutton and Chen are identical for Ni and Cu except for the overall potential scaling factor, ϵ. This means that the phonon frequencies calculated for Ni in this pa-

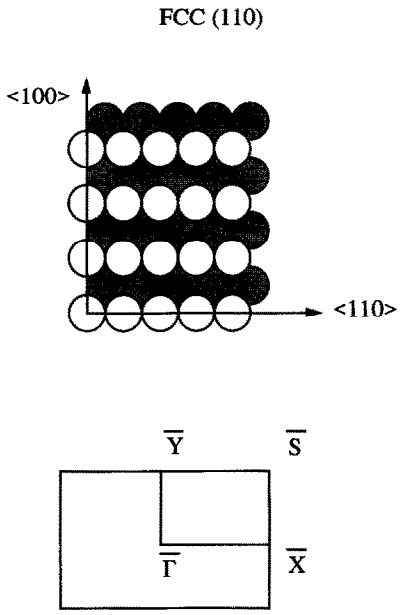

Fig. 1. Arrangement of surface atoms for a fcc (110) surface. The direct lattice (top) and the surface Brillouin zone (bottom) are shown along with the major high-symmetry points. In this paper, the x-direction corresponds to the $\langle 110 \rangle$ direction, the y-direction corresponds to the $\langle 100 \rangle$ direction, and the z-direction is out of the plane of the paper.

per can be multiplied by $\epsilon_{Cu}/\epsilon_{Ni} = 0.7880$ to obtain the results for Cu [23]. In a previous paper we have used these potential parameters to calculate the (100), (110), and (111) surface phonon spectral densities for Ni and Cu at 300 K and have compared these results to experimental measurement of the surface phonon dispersion curves [23]. What makes FS potentials so valuable is that the surface bonding changes, i.e., the stiffening of the interplanar force constant or the incorporation of an intraplanar stress term, are automatically included in the form of the FS potential.

The real-space geometry and corresponding surface Brillouin zone for the (110) surface is shown in fig. 1. The simulation used 3100 atoms, with a 10×10 arrangement of atoms located in each layer (x- and y-directions) and a total of 31 layers (z-direction). At the beginning of the simulation the initial lattice positions were set taking into account the thermal expansion of the fcc lattice for the desired simulation T, as given by Chen et al. [16]. The slab layers were not relaxed to the minimum potential energy at $T = 0$ K. Once the simulatin is started this non-relaxed potential energy increases the intensity of low vibrational modes near $\bar{\Gamma}$ which damp slowly at low T and faster at high T. This is the origin of the small T and potential energy oscillations and the root mean square displacements not equaling 0.0 at $T = 0$ K in our previous Lennard-Jones paper [19]. These oscillations in T and potential energy are less pronounced at $T \geq 200$ K. For this reason only T from 200 to 700 K were used in the fits shown in tables 1 and 2. These long wavelength oscillations have no effect on the short wavelength vibrations presented in the results section. This was evident by the nearly identical fits obtained by including and excluding the $T =$ 50–150 K data.

The equations of motion were integrated using a 7th-order predictor–corrector method [24]. For most simulations ($T = 150$–700 K) an integration time step of 2.5 fs was chosen. This choice of time step gives an energy resolution of 0.404 meV when a total of 4096 time steps are used. This choice of time step also conserves the total energy of the system during the simulation run to better than 1 part in 10000. For simulations with $T \leq 100$ K an integration time step of 5.0 fs was used, while 2.0 fs was used for simulations with $T \geq 700$ K.

All spectral densities, $f^{\alpha\beta}(\bar{A}; l_z, \omega)$, were calculated after equilibrium was attained, i.e. $\alpha(t) = 5/3$ [19,20]. For high-T simulations ($T = 600$ to 700 K) up to 60 $f^{\alpha\beta}(\bar{Q}; l_z, \omega)$ were added together to resolve phonon lineshapes. These runs were taken consecutively, with the final coordinates from the previous runs providing the initial coordinates for the following run. In this paper we present simulation results only for $T \leq 700$ K, since starting at 750 K the surface atoms were found to move out from their initially assigned lattice positions and exhibit diffusive motion.

2.1. Mean square displacements and surface stress

Temperature-dependent MS displacements along all three principal directions were calculated for the first, second, and third layers, as

Table 1
The change in the mean-square displacements (MSD) as a function of T for Ni(110)

Layer	x-direction		y-direction		z-direction	
	m_1	m_2	m_1	m_2	m_1	m_2
1	3.67	2.33	3.26	5.59	3.97	0.95
2	2.64	1.31	2.39	1.96	4.36	1.30
3	2.48	0.97	2.28	1.31	3.47	0.27
Bulk	2.10	0.59	2.05	0.75	2.06	1.01

The MSD were fit to a quadratic functional form, where MSD-$m_1^* T + m_2^* T^2$, L in units of 10^{-5} Å^2 K^{-1}, and Q in units of 10^{-8} Å^2 K^{-2}. MSD was assumed to be 0 at $T = 0$ K. m_1 in units of 10^{-5} Å^2 K^{-1}. m_2 in units of 10^{-8} Å^2 K^{-2}.

well as the bulk, from $T = 200$–700 K. The MSD were assumed to be equal to 0 at $T = 0$ K. The MSD increased linearly at low T and quadratically at high T. The MSD were fit to the equation, MSD $= m_1^* T + m_2^* T^2$, with the values of m_1 and m_2 shown in table 1. Previously in our LJ paper we found that the root mean square displacements were linear with T [20], implying that the MSD presented in the LJ paper had a quadratic dependence on T and could be plotted using the above formula. Interesting results below 600 K are: (i) For the first layer, displacements along the $\hat{z}$-direction are smaller than for either of the in-plane directions. This is a direct consequence of using the FS model potential, which increases the charge density between the first and second layer [21–23]. Similar observations for first layer RMSD were also observed in other MD simulations of Ni(110) [16]. (ii) From table 1, significant deviations from linear T dependence, i.e., the onset of curvature in the MSD versus T plots, appears most strongly in the first layer results along the $\hat{y}$-direction where the value of $m_2 = 5.59 \times 10^{-8}$ Å^2 K^{-2} is the largest. This result is intuitively reasonable given that the $\hat{y}$-direction corresponds to displacements which are perpendicular to the atomic rows on the (110) surface. (iii) Displacements along the $\hat{z}$-direction for the second layer are larger than for the first (surface) layer. This implies that the surface atoms are held more rigidly in the $\hat{z}$-direction than those in the the second layer. As discussed in the next section, this result has important consequences for the temperature dependence of the surface phonon spectral density, i.e., phonon energies and linewidths. In addition, this result offers insight into the types of atomic displacements that are ultimately responsible for the creation of defects, especially adatom–vacancy pairs [10,11,16].

Stress tensor terms were also calculated following Needs [25]. Lehwald et al. have added stress terms to a nearest-neighbor force constant model to explain the surface lattice dynamics of Ni(110) [26]. No unusual changes were observed in the stress tensors as a function of T, which decreased smoothly and nearly linearly before the onset of defect formation at ~ 750 K. For further discussion of this point we refer the reader to our earlier work which utilized Lennard-Jones-based potentials [20]. The stress is largest for the $\hat{x}\hat{x}$-tensor which indicates a strong compressive stress along the atomic rows or the $\langle 110 \rangle$ direction. A smaller compressive stress also exists perpendicular to the atomic rows. This differs from the results with LJ potentials, is real, and is due to the many-body nature of the FS potential.

2.2. Phonon spectral densities

The values of $f^{\alpha\beta}(\bar{Q}, l_z, \omega)$ as a function of T were calculated as previously discussed [19,20]. For the remainder of this section we will focus on the results at $\bar{Y}$ rather than $\bar{X}$ as the former are not complicated by the promixity of underlying bulk contributions.

Illustrative surface phonon spectral density plots at $\bar{Y}$ for three temperatures are shown in fig. 2. These peaks correspond to the $\hat{z}$-polarized S_3 surface mode or Rayleigh wave for the (110) surface [27]. As T increases, these spectral densities display a shift to lower frequency and an increase in linewidth, as shown in figs. 3 and 4, respectively.

The T-dependencies of the phonon frequencies and linewidths have been compiled in table 2. In this table the first column denotes the reciprocal lattice point, either $\bar{X}$, $\bar{Y}$, or $\bar{S}$, where the spectral densities were calculated. The surface phonon modes are listed according to the nomenclature introduced by Allen, Alldredge and the Wette [27] in the second column. The third

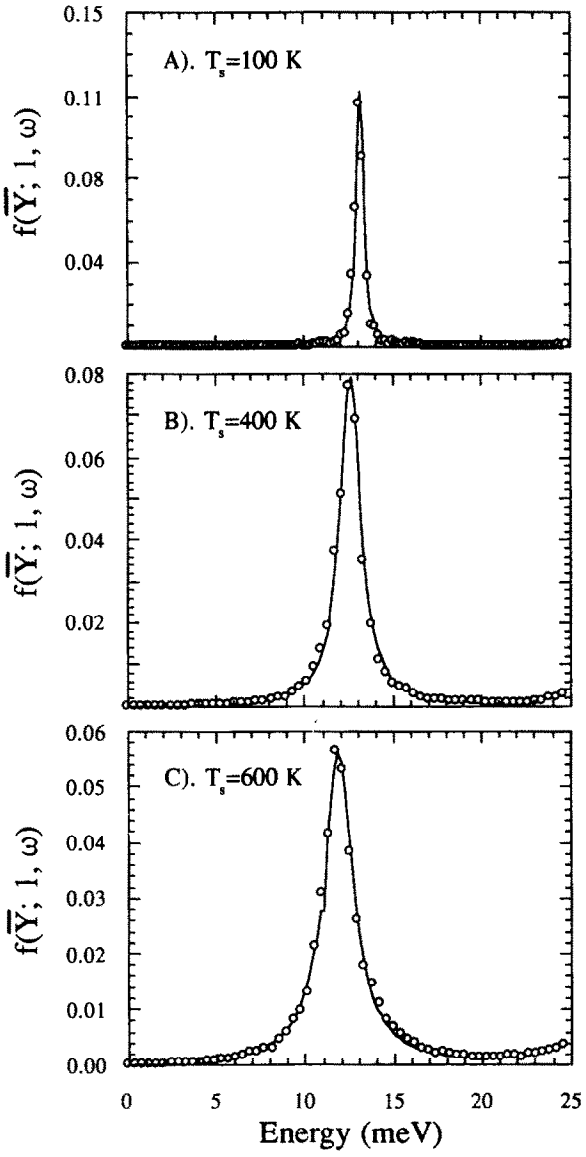

Fig. 2. Calculated z-polarized surface phonon spectral density at $\bar{Y}$ for three surface temperatures: (A) 100 K, (B) 400 K, and (C) 600 K. The open circles are the values of $f(\bar{Y}; l, \omega)$ and the solid line is a fit to these values are described in the text.

column lists the layer for which the mode as a maximum intensity (either the first or second layer). The fourth column gives the principle polarization of the surface mode. The polarization is the value of $\alpha = \beta$ which is used to calculate the phonon spectral density. The fifth column

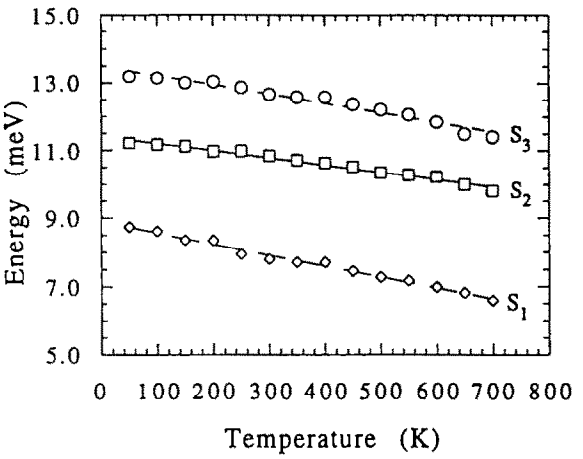

Fig. 3. Temperature dependence of phonon frequencies at $\bar{Y}$ for x-polarized (open squares), y-polarized (open diamonds), and z-polarized (open circles) surface phonons.

contains the value of the fitted $T = 0$ K phonon frequency, E_0, in units of meV. The value of E_0 ($T = 0$ K) was calculated from a linear least-squares fit to the T-dependence ($T \geq 200$ K) of the phonon frequencies, and is the $T = 0$ K intercept from this fit. These values for E_0 are only appropriate for Ni. To obtain the values for Cu each of the Ni E_0 values must be multiplied by $\epsilon_{Cu}/\epsilon_{Ni} = 0.7880$, as previously discussed. The sixth column contains the negative of the slope of this fit, $-\Delta E_{E_0}/\Delta T$, which has been normalized by the value E_0 ($T = 0$ K) so that the slopes can

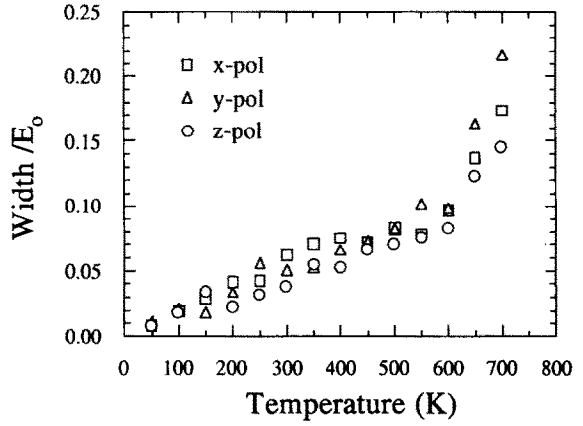

Fig. 4. FWHM of the surface phonon spectral densities at $\bar{Y}$ as a function of T for x, y, and z-polarizations. The FWHM of the phonon mode has been divided by the frequency of the corresponding mode at $T = 0$ K (see table 2).

be evaluated independently of the initial frequency [20]. The seventh column contains the slopes, $\Delta W_{E_0}/\Delta T$, derived from linear fits of the phonon linewidth, W, for $T = 200$ to 600 K. These values have also been divided by E_0. The eighth column contains the slopes, $\Delta E^*_{E_0}/\Delta T$, from linear fits of W divided by E_0 ($T = 0$ K) for $T = 600$ to 700 K. Since only three points are used to calculate these slopes, they should also be used to gain a rough estimate of the change in the rate at which the linewidth increase with increasing temperature. Because only three points were calculated in this temperature range we did not fit the T-dependence to a quadratic curve as we did in our earlier work involving LJ potentials [20]. Also notice that some of the modes either do not appreciably change slope from 600 to 700 K, or have fit parameters that are ambiguous so that no value of $\Delta W^*_{E_0}/\Delta T$ is given. In the ninth column, the ratio of $\Delta W^*_{E_0}/\Delta T$ to $\Delta W_{E_0}/\Delta T$ is shown. This ratio allows one to quickly assess the importance of anharmonic effects at elevated temperatures (600–700 K), i.e. the larger the value of this ratio the larger the influence of anharmonicity for a particular phonon mode.

The linewidths at $\bar{Y}$ for the S_1 ($\hat{y}$-polarization), S_2 ($\hat{x}$-polarization), and S_3 ($\hat{x}$-polarization) are shown in fig. 4. Each of these modes show qualitatively the same linear increase in linewidth as T is increased up to 600 K, followed by a crossover to T^2 dependence. As seen in fig. 4, at these higher temperatures a more pronounced linewidth increase occurs for S_1 ($\hat{y}$-polarization) as compared to either the other in-plane direction

Table 2
Changes in the phonon frequencies, E, and width, W, as a function of T

$\bar{Q}$	Mode	Layer	x, y, z	E_0 ($T = 0$ K) [a]	$-\Delta E_{E_0}/\Delta T$ [b]	$\Delta W_{E_0}/\Delta T$ [c]	$\Delta W^*_{E_0}/\Delta T$ [c]	Ratio
$\bar{X}$	S_1	1	z	14.24	0.160	0.131	–	–
	S_7	1	x	23.42	0.016	0.298	0.78	2.6
	S_2	1	y	17.33	0.176	0.128	1.50	11.7
	S_1	2	z	13.92	0.120	0.138	–	–
	SR	2	x, y	22.60	0.093	0.190	1.05	5.5
$\bar{Y}$	S_1	1	y	9.03	0.381	0.168	1.17	7.0
					(0.335) [d]	(0.411)	–	–
	S_2	1	x	11.53	0.200	0.166	0.77	4.6
					(0.202)	(0.205)	–	–
	S_3	1	z	13.66	0.219	0.136	0.62	4.5
					(0.181)	(0.118)	(0.572)	4.9
					{0.177} [d]	{0.235}	–	–
	S_5	1	y	21.23	0.161	0.159	1.55	9.8
					(0.162)	(0.172)	–	–
	SR	2	x	16.00	0.153	0.169	0.82	4.9
	S_3	2	y	13.55	0.198	0.127	1.95	15.4
	S_1	2	z	8.87	0.327	0.174	1.99	11.4
	S_5	2	z	21.36	0.123	0.173	2.34	13.5
$\bar{S}$	S_1	1	y	12.93	0.198	0.184	1.83	10.0
	S_2	1	z	14.48	0.160	0.113	1.80	15.9
	SR	1	x	25.73	0.023	0.259	–	–
	S_1	2	x	12.74	0.145	0.177	1.96	11.1
	S_2	2	y	14.49	0.015	0.228	2.00	9.0

[a] E_0 ($T = 0$ K) in units of MeV.
[b] $-\Delta E_{E_0}/\Delta T$ in units of 10^{-3} K^{-1}.
[c] $\Delta W_{E_0}/\Delta T$ and $\Delta W^*_{E_0}/\Delta T$ in units of 10^{-3} K^{-1}.
[d] Values in parentheses are from ref. [10], and values in braces are from ref. [11].

or along the surface normal. The dramatic increase in linewidth beginning near 600 K provides clear evidence for the increased influence of anharmonicity at elevated temperatures, approximately 150° before the onset of defect creation at the surface. The values for the first layer $\hat{x}$-, $\hat{y}$-, and $\hat{z}$-polarized linewidths at $\overline{X}$ have also been examined. Similar trends are seen as at $\overline{Y}$, with the $\hat{y}$-polarized S_3 mode changing from T to T^2 behavior above 600 K.

3. Discussion

In the previous section a number of temperature-dependent simulation results were presented. We begin this section with a discussion of the differences between these Finnis–Sinclair (FS) results and our earlier simulations which employed Lennard-Jones (LJ) potentials [19,20]. In this section we also compare our FS-based findings to the results of previous calculations which used EAM and EMT potentials to examine the T-dependencies of the surface phonon frequencies and linewidths for Cu(110) at $\overline{Y}$ [10,11]. Finally, we also discuss the significance of the FS findings in relation to surface roughening and the influence of anharmonicity at elevated temperatures, including a comparison of our results to the recent temperature-dependent HREELS measurements of Baddorf and Plummer on Cu(110 [12,13].

The emergence of non-central potential models such as the Finnis–Sinclair, EMT, and EAM have been essential for both predicting surface phenomena and for developing simple physical models of the bonding changes that occur at surfaces. These density functional methods make the assumption that the total energy of the solid can be described as a sum of a repulsive two-body pair potential and a many-body cohesive potential. A notable success has been the prediction of a reduction in the first-to-second interlayer spacing as compared to bulk values. Here electronic charge redistribution at the surface lowers the kinetic energy of the surface electrons, i.e., a "smoothing" of the surface electronic states occurs [28]. As a result of this smoothing, the density of electronic states at the surface is compressed in energy which increases the amount of cohesive bonding at the surface [28].

Our simulations using FS model potentials produce results qualitatively similar to simulations which use EAM or EMT potentials since the ansatz for these potentials, as stated above, is basically the same [28]. We have previously shown that the FS model potential somewhat underestimates the many-body density term used to scale the forces at the surface [23]. This underestimation produces surface phonon frequencies which are semi-quantitative, but systematically too low, when compared to experimentally determined values. This decreases the temperature range at which surface phonon linewidth changes are observed first, but should not change the overall description of the Ni(110) or Cu(110) surfaces. (In our previous work we found that the overall agreement between the calculated surface phonon frequencies and the experimentally measured values was in fact better for the (110) than either the (100) or (111) surfaces [23].)

The major differences between simulations which use FS and LJ potentials are due to the presence of a many-body term in the former. For example, manifestations of the importance of this many-body term can be seen in the qualitative differences which appear in the calculated MS displacements. For LJ potentials the RMSD decrease monotonically as a function of layer number, with the RMSD along the $\hat{y}$-direction decreasing faster than for either the the $\hat{x}$- or $\hat{z}$-directions [20]. This is in contrast to the FS results, where although the same monotonic trend is seen for the in-plane modes, along the $\hat{z}$-direction we find that the second layer's MSD are *greater* than those for the first layer. Similar observations have been reported for Ni(110) using the EAM [16].

The above implies that first layer atoms are held more tightly in the $\hat{z}$-direction than are those in the second layer. For this reason no increase in step density or number of adatom–vacancy pair defects is expected, or observed, in EAM and EMT simulations up to 70% of the melting T of Cu(110) or Ni(110) [10,11,16]. We also witnessed the onset of defect creation at 750

K when simulating Ni(110), but did not extensively study the number or type of defects created. The onset of defects at this relatively low T is due to the previously discussed underestimation of the many-body density term. We also reiterate for the sake of clarity that temperatures cited in this paper are with respect to Ni – in order to convert the temperature to the right scale for Cu one needs to multiply T by 0.788.

In addition to the above differences in MSD behavior for simulations using FS and LJ potentials, structural differences also appear. The most obvious one is that the first to second layer spacing is larger than in the bulk when LJ potentials are used – in contrast to the FS results, as well as experiment. This is a consequence of the reduced coordinated at the surface and, for LJ solids, the absence of a functional dependence of the binding potential on atomic density.

We also note that the temperature at which anharmonicity begins to influence the lattice dynamics is significantly different for FS potentials compared to LJ potentials, with LJ solids making the T to T^2 transition at approximately 0.20 times the melting temperature of the solid (and becoming quite apparent by $0.30T_m$, as shown in fig. 5 of ref. [20]), whereas for the FS solid this occurs above 600 K, at ~ 0.4–0.5 times the melting temperature of the simulated solid [29]. (For potential models which do not underestimate the many-body binding potential, the T to T^2 transition can occur at temperature even higher than 0.4–$0.5T_m$.)

The extent to which surface phonon frequencies decrease as T is increased is summarized in column 6 of table 2. In this column the rate of decrease in phonon frequency has been divided by the phonon frequency at 0 K. This was done so that the results for various first and second layer modes could be compared directly. In previous simulations using LJ potentials we attempted to quantify the relative contribution to these frequency decreases originating from thermal expansion of the lattice and anharmonic terms for LJ potentials [20] (also examined by Ditlevsen et al. for EMT potentials [11]). We found that the anharmonic contribution to the frequency decrease on the (100) and (111) surfaces was usually stronger for modes localized to the surface – a reasonable observation since these vibrations are more strongly affected by thermally excited atomic displacements. However, it was harder to separate these contributions for the (110) surface since the atomic motions of the modes tend to penetrate deeper into the bulk than for modes on the other, more densely packed, surfaces [20]. Notice in column 6, however, that most of the modes tend to have frequency decreases in the range 0.14–0.20, or equal to 0.0, implying that thermal expansion can account for most of the frequency decrease. The one exception to this is the S_1 at $\bar{Y}$ and $\bar{S}$ which has the largest frequency decrease of all modes. This mode has a large in-plane shear vertical motion, and thus samples the anharmonic potential to a greater extent than other modes as T is increased.

It is clear from figs. 2 and 4 that the linewidth for the $\hat{z}$-polarized surface phonon spectral density at $\bar{Y}$ increases as T is increased. In fig. 4 we furthermore see that the linewidth increases linearly from 200 to 600 K, and that from 600 to 700 K this increase becomes much more rapid. In our earlier simulation studies using LJ potentials [20] we attributed this increased sensitivity of linewidth to surface temperature to the "turning on" of higher order phonon–phonon coupling terms [17,18,30]. When these higher order phonon–phonon coupling terms become important in the dynamics, the surface phonon linewidth will begin to increase proportionally to T^2 [17,18,30]. We point out that the modes with the largest increase in linewidth are the S_2 mode at $\bar{X}$, the second layer modes at $\bar{Y}$, and the first layer modes at $\bar{S}$. The reason that the second layer modes at $\bar{Y}$ exhibit this behavior rather than those in the first layer can be traced to the relative RMSD along the $\hat{z}$-direction, i.e., the second layer atoms have larger excursions from their mean positions than do the first layer atoms, and therefore sample more of the anharmonic potential.

Table 2 also shows the T dependencies of the surface phonon frequency and linewidth for Cu(110) at $\bar{Y}$ calculated using the EAM in (in parentheses) [10], and the EMT (in braces) [11]. We find excellent overall agreement between our

simulation results and those calculated using both the EAM and EMT methods [10,11]. Specifically, there is excellent agreement between our results for the S_3 mode (Rayleigh wave) and the EAM results at $\overline{Y}$ [10]. Both calculations predict that this mode should have a rapid increase in linewidth caused by anharmonicity, and that the ratio of this anharmonic increase at high T should be 4.5–4.9 times the rate of increase at low T.

Furthermore, good agreement is also found when the T dependence of the simulated S_3 at $\overline{Y}$ is compared with the HREELS data of Baddorf and Plummer [12,13]. Because the experiment was conducted on Cu(110) the value of E_0 listed in table 2 has to be multiplied by $\epsilon_{Cu}/\epsilon_{Ni} = 0.7880$. The value of $\Delta E_{E_0}/\Delta T$ for Cu(110) does not need to be multiplied by $\epsilon_{Cu}/\epsilon_{Ni}$ since T also scaled by $\epsilon_{Cu}/\epsilon_{Ni}$ [23]. Baddorf and Plummer report a linear fit to the frequency of the S_3 mode of $E = 12.38 - 0.0020T$ [13]. Using the values in table 2 we calculate a frequency dependence of $E = 10.62 - 0.00209T$. The frequency decreases of these fits are identical within experimental and simulation error. This can be easily explained since the decrease in energy of S_3 as a function of T is most closely related to thermal expansion of the lattice. As this is primarily a bulk effect the simulation results should agree quite well with experiment, since for each T the lattice expansion was accounted for. E_0 differs due to the previously discussed underestimated of the many-body binding term when using the FS potential.

The agreement between the mode's calculated linewidth and the experimental value is not as good. Baddorf and Plummer report a linear fit to the linewidth dependence of the phonon mode of $W = 4.56 - 0.0060T$ [13]. Using the value of table 2, we get $W = 0.00 - 0.00148T$. Because at low T the dynamics can be described using the harmonic approximation, there are no mechanisms to limit the surface phonon lifetime, hence the surface phonon linewidth should be infinitely narrow. The finite linewidth that Baddorf and Plummer measured at low T must therefore be due to the instrumental resolution of the HREELS [13]. Clearly more experiments will have to be done to provide a better data base for comparison between experiments and the results presented in this paper.

4. Conclusions

To summarize, molecular dynamics simulations have been performed for the (110) surfaces of Ni and Cu using Finnis–Sinclair model potentials. Our calculations have explicitly examined the T-dependencies of the MS displacements, stress tensors, and first and second layer surface phonon spectral densities. For the first layer we find that the MSD along the ⟨110⟩ direction are larger than for either the other in-plane direction or along the surface normal. We also find that displacements along the surface normal are always larger in the second layer than are those for the first layer. This is a direct consequence of using the FS potential, which naturally redistributes interfacial charge density between the first and second layers. Our results indicate that the surface lattice dynamics of both Ni(110) and Cu(110) are sensitive to anharmonic effects well below their respective melting temperatures. Moreover, these calculations have assessed the relative contributions of anharmonicity and defect formation to the surface dynamics of these materials at intermediate temperatures, and have shown that anharmonic effects successfully account for HREELS [12,13] and elastic He scattering [9] measurements in this temperature regime. This is primarily due to the "turning on" of higher order phonon–phonon coupling terms at intermediate temperatures, in excess of ~ 600 K for Ni and ~ 475 K for Cu, as indicated by a change from linear to quadratic in the temperature dependence of phonon linewidth. This change from linear to quadratic dependence occurs for a majority of the modes examined in this paper. We close by emphasizing that the temperature at which this change in phonon linewidth behavior occurs is approximately 150° lower than that needed for the creation of defects at the surface, supporting the conjecture that the faster than Debye–Waller specular intensity attenuation observed in several diffraction studies is due to the influence of anharmonicity in the surface potential, and not to the onset of roughening.

Acknowledgements

We would like to thank P. Knipp and D. Padowitz for many useful discussions. This work was supported, by the National Science Foundation Materials Research Laboratory at the University of Chicago and the Air Force Office of Scientific Research.

References

[1] S.G.J. Mochrie, Phys. Rev. Lett. 59 (1987) 304.
[2] G.A. Held, J.L. Jordan-Sweet, P.M. Horn, A. Mak and R.J. Birgeneau, Phys. Rev. Lett. 59 (1987) 2075.
[3] B. Salanon, F. Fabre, D. Gorse and J. Lapujoulade, J. Vac. Sci. Technol. A 6 (1988) 655.
[4] J. Lapujoulade, Surf. Sci. 178 (1986) 406.
[5] U. Breuer, O. Knauff and H.P. Bonzel, Phys. Rev. B 41 (1990) 10848.
[6] J.W.M. Frenken, R.J. Hamers and J.E. Demuth, J. Vac. Sci. Technol. A 8 (1990) 293.
[7] H. Yang, T. Lu and G. Wang, Phys. Rev. B 43 (1991) 4714.
[8] Y. Cao and E.H. Conrad, Phys. Rev. Lett. 64 (1990) 447.
[9] P. Zeppenfeld, K. Kern, R. David and G. Comsa, Phys. Rev. Lett. 62 (1989) 63.
[10] L. Yang and T.S. Rahman, Phys. Rev. Lett. 67 (1991) 2327.
[11] P.D. Ditlevsen, P. Stoltze and J.K. Nørskov, Phys. Rev. B 44 (1991) 13002.
[12] A.P. Baddorf and E.W. Plummer, J. Electron Spectrosc. Rel. Phen. 54/55 (1990) 451.
[13] A.P. Baddorf and E.W. Plummer, Phys. Rev. Lett. 66 (1991) 2770.
[14] R. Franchy, M. Wuttig and H. Ibach, Surf. Sci. 203 (1988) 489.
[15] K. Kern, U. Becher, P. Zeppenfeld, G. Comsa, B. Hall and D.L. Mills, Chem. Phys. Lett. 167 (1990) 362.
[16] E.T. Chen, R.N. Barnett and U. Landman, Phys. Rev. B 41 (1990) 439.
[17] G. Armand and P. Zeppenfeld, Phys. Rev. B 40 (1989) 5936.
[18] G. Armand, D. Gorse, J. Lapujoulade and J.R. Manson, Europhys. Lett. 3 (1987) 1113.
[19] D.D. Koleske and S.J. Sibener, Surf. Sci. 268 (1992) 406.
[20] D.D. Koleske and S.J. Sibener, Surf. Sci. 268 (1992) 418.
[21] M.W. Finnis and J.E. Sinclair, Phil. Mag. A 50 (1984) 45.
[22] A.P. Sutton and J. Chen, Phil. Mag. Lett. 61 (1990) 139.
[23] D.D. Koleske and S.J. Sibener, Surf. Sci. 290 (1993) 179.
[24] W.E. Milne, Numerical Solutions of Differential Equations (Dover, New York, 1970).
[25] R.J. Needs, Phys. Rev. Lett. 58 (1987) 53.
[26] S. Lehwald, F. Wolf, H. Ibach, B.M. Hall and D.L. Mills, Surf. Sci. 192 (1987) 131.
[27] R.E. Allen, G.P. Alldredge and F.W. de Wette, Phys. Rev. B 4 (1971) 1661.
[28] A.E. Carlsson, in: Solid State Physics, Eds. H. Ehrenreich and D. Turnbull (Academic Press, New York, 1990) p. 1.
[29] The estimate of the melting temperature for FS potentials was based on the observation that the roughening transition temperature occurs at approximately half of the melting temperature for fcc metals. We begin to see atoms moving out of their initially assigned lattice positions at 750 K in this paper, and assume this to be the start of roughening. For LJ potentials the roughening transition begins to occur at 0.45 times the melting T, in rough agreement with this crude method of T_m estimation.
[30] G. Armand, J.R. Manson and C.S. Jayanthi, Phys. Rev. B 34 (1986) 6627.